Journal of Physics: Materials

PAPER

Optical behaviour of γ-black $CsPbI_3$ phases formed by quenching from 80 °C and 325 °C

Salvatore Valastro[1,3], Giovanni Mannino[1], Emanuele Smecca[1], Salvatore Sanzaro[1], Ioannis Deretzis[1], Antonino La Magna[1], Ajay Kumar Jena[2], Tsutomu Miyasaka[2] and Alessandra Alberti[1,*]

[1] CNR-IMM, Zona Industriale Strada VIII n.5, 95121 Catania, Italy
[2] Graduate School of Engineering and Faculty of Medical Engineering, Toin University of Yokohama, 1614 Kurogane-cho, Aoba, Yokohama, Kanagawa 225-8503, Japan
[3] Dipartimento di Fisica e Astronomia, Università di Catania, Via S. Sofia 64, 95123 Catania, Italy
* Author to whom any correspondence should be addressed.

E-mail: alessandra.alberti@imm.cnr.it

Keywords: inorganic perovskites, solution processing, thin films, stability

OPEN ACCESS

RECEIVED
28 December 2020

REVISED
19 March 2021

ACCEPTED FOR PUBLICATION
21 April 2021

PUBLISHED
11 May 2021

Abstract

The orthorhombic γ-black phase of $CsPbI_3$ is well-known to be unstable at room temperature and strategies are needed to counteract its transformation tendency. In this paper we compare γ-black $CsPbI_3$ thin films (∼80 nm) formed via two different routes: a fast quenching of the cubic α-phase from 325 °C (HT-γ) or spontaneously cooling the layer from 80 °C (LT-γ). The successful application of the second procedure is allowed by the use of a mother solution containing Europium with an Eu/Pb ratio as small as 5%. This has been indeed used to form both LT-γ and HT-γ thin films. The phase transition during the heating and cooling pathways is followed *in situ* by spectroscopic ellipsometry and x-ray diffraction analyses. We demonstrate that both γ-black phases exhibit the same absorption features and critical points as depicted in very details by the dielectric functions. Minor differences can be found in the intensity of the absorption coefficient, assigned to an improved lattice quality in the layer that has experienced the high temperature path. On the other hand, α-black and δ-yellow phases show different critical points in the optical transitions. Besides providing benchmarking optical parameters to discriminates the different phases, we demonstrate that the LT-γ phase closely competes with the HT-γ counterpart during stress tests for stability, with the first one more suited for tandem monolithic architectures that require thermal treatments under 200 °C.

1. Introduction

Two-terminal monolithic perovskite-on-silicon tandem cells represent the most promising innovative photovoltaic devices for a near-term large-scale commercialization [1, 2]. This technology allows reaching high efficiencies (the current record is 29.1% [3]) coupling a relatively wide bandgap perovskite solar cell (top cell) with a silicon solar cell (bottom cell) which absorb in different and complementary regions of the solar spectrum. Hybrid organic/inorganic perovskites such as methylammonium lead iodide ($MAPbI_3$), formamidinium lead iodide ($FAPbI_3$) and methylammonium (MA)–formamidinium (FA) mixed perovskite are the most used and known perovskite absorber layers. If on the one hand, the presence of organic elements (MA, FA) as the A-site cation of the perovskite crystal structure is the key to achieve high efficiency, on the other hand, the organic cations are often weak links due to their intrinsic instability when they are exposed to humidity, elevated temperatures and solar light [4–9].

The structural instability of hybrid perovskites has moved the attention also toward all-inorganic perovskite materials, in which the organic cation is replaced by an inorganic cation like Cs. Cesium lead iodide ($CsPbI_3$) with bandgap of ∼1.73 eV is a well-matching candidate for silicon-perovskite tandem solar

cells. The $CsPbI_3$ can exist in four phases: cubic phase (α), tetragonal phase (β), and two orthorhombic phases (γ and δ). The δ orthorhombic, well-known as 'yellow phase', is a non-active non-perovskitic phase, indeed unusable for photovoltaic applications. The α, β and γ phases, in contrast, have a perovskite structure that exhibits the photovoltaic behaviour: they are better known as 'black phases'. Unfortunately, α, β and γ are stable at high temperatures (>RT) [10, 11] whilst metastable at room temperature (RT), implying that they spontaneously turn to the yellow orthorhombic phase under ambient conditions or during operation [12, 13].

For the abovementioned reason, the stabilization of a perovskitic $CsPbI_3$ black phase at room temperature is the main technological challenge. In previous years, several methods like modifying processes [14], additives [15] and tuning the tolerance factor of $CsPbI_3$ [16] by elemental doping [17–23] have been attempted to extend the stability of the black α and β-phases towards operative conditions. All of these approaches require a thermal annealing of the $CsPbI_3$ film at temperature >250 °C, making its integration in silicon-perovskite tandem solar cells unfeasible. As a matter of fact, in monolithic tandem devices, the perovskite solar cell is deposited directly on the silicon cell and low-temperature processes (<200 °C) are needed in order to not damage the underlying layers of the bottom cell [24].

Additionally, the orthorhombic γ-phase, which has similar optoelectronic properties to α-phase [25], can be obtained at low temperature through different strategies [26]. Among the others, the addition of hydroiodic acid (HI) [27–29], organic ligands (phenethylamine [13], ethylenediamine [30], sulfobetaine zwitterion [31], organic ammonium cations [32], ethanediamine [33]) or elemental doping (germanium [34], bismuth [35, 36], strontium [37], indium [38], calcium [39]) can facilitate the formation of stable orthorhombic $CsPbI_3$ phase at low annealing temperature, acting on the morphology of the perovskite film, especially on the dimension of grains during the crystallization process [40–42]. The interplay between surface energy cost and bulk energy gain makes the black and yellow phases to compete in the range of small grain sizes. Under those morphological conditions, the $CsPbI_3$ γ-phase can become thermodynamically more stable than the δ-phase [43].

Among the possible stabilization processes of $CsPbI_3$ black phase based on the elemental doping, the incorporation of Europium atoms into $CsPbI_3$, reported by Miyasaka *et al* [44], is considered a promising solution for obtaining a stable black phase. The black γ-phase of $CsPbI_3$:*x*Eu is obtained after annealing the spin-coated layer at low temperature (85 °C) for 15 min. The stability of the black phase (stored in dark and ambient condition with less than 20% relative humidity) changes with Eu concentration: higher Eu content results in longer durability of the black phase. The best device efficiency of ∼6% was achieved when Eu/Pb = 5%.

Following this benchmarking method, in this paper, we form a thin γ-$CsPbI_3$ phase on glass substrates at a temperature of 80 °C (LT-γ black) using a relative amount of Pb/Eu = 5% to investigate the optical and dielectric properties of the layer by spectroscopic ellipsometry in the range of 1–6 eV. We study the phase transitions that occur while progressively varying the temperature from 30 °C to 325 °C and after quenching to 30 °C under dry nitrogen environment through sequential *in situ* analyses. We compare the optical behaviour of the LT-γ black phase with the one of the cubic α-phase obtained at 325 °C through the Critical Points (CPs) analysis, which provides the transition energies by fitting simultaneously the second derivatives of the real and imaginary part of the dielectric function [45]. We additionally highlight the effect of the cooling speed from 325 °C to room temperature to eventually produce a HT-γ black phase (∼2.5 °C min^{-1} or ∼100 °C min^{-1}). The optical behaviour of the HT-γ black phase is finally compared to the one of the LT-γ black phase cooled from 80 °C, all done on the same sample.

2. Materials and methods

2.1. Perovskite film fabrication

A solution of 1 M PbI_2 (Tokyo Chemical Industry) and 1 M CsI (Tokyo Chemical Industry) was prepared by mixing them in a composite solvent made of DMF and DMSO (3:1 v/v). $EuCl_3$ (Sigma-Aldrich) solution of 0.1 M concentration was made in same mixed solvent of DMF and DMSO (3:1 v/v). The solutions were stirred at room temperature for 1 h. Then, 1 ml of the PbI_2/CsI solution was mixed with 0.5 ml of the $EuCl_3$ solution to reach the desired stoichiometry and then stirred for 1 h. The perovskite film was deposited by spin-coating the precursor solution on glass substrates in two steps: 1000 rpm for 10 s followed by 5000 rpm for 25 s in ambient environment. The $CsPbI_3$ prepared with Eu/Pb = 5% film was then annealed at 80 °C on a hot plate for 1 min and cooled to 30 °C at 0.5 °C–1 °C s^{-1} to form the black LT-γ phase. The final layer on glass has a thickness of ∼80 nm. The sample is hereafter called $CsPbI_3$:5Eu. The composition of the mother solution was chosen according to the results of paper [44], on the basis of the best solar cell performances achieved.

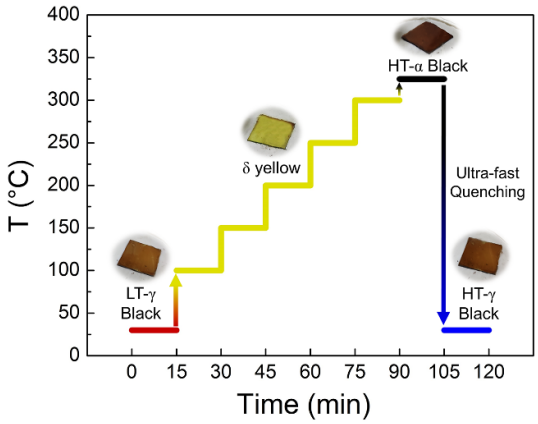

Figure 1. Schematic of the thermal cycle with the observed crystallographic phases. The starting phase was produced after spin coating, annealing to 80 °C for 1 min and cooling down to 30 °C. Each step covers 50 °C and the whole cycle is done under dry N_2 in order to focus on the intrinsic behaviour of the different phases.

2.2. Spectroscopic ellipsometry

We used a V–VASE, J A Woollam spectroscopic ellipsometry equipped with an autoretarder for optical characterization. Ellipsometric data have been collected at different angles below and above the Brewster angle of the glass substrate, over a wide range of wavelengths 245–1240 nm (1–5 eV) with step of 10 nm or less (5 nm) depending on the curve steepness. The optical model is a three layer model that take into account the optical constants of the glass substrate, the perovskite layer and the surface layer needed to simulate the layer roughness. Within the effective model approximation this last layer is assumed to be made 50% of the upper layer (air) and 50% of the lower layer (perovskite). The presence of a transparent substrate has been properly taken into account including the possibility that part of the light hits the backsurface of the glass slide. We build a Kramers–Kronig consistent optical model based on multiple (7) Tauc-Lorentz oscillators to fit experimental data (psi and delta) and determine the real and imaginary part of the dielectric function. Measurements have been collected using a slightly overpressurized N_2 filled chamber in order to prevent perovskite degradation in air. The cell setup allowed to vary the temperature in the range 30 °C–325 °C with an Instec MK100 heater/cooler system with an accuracy of 0.1 °C. Although it is known that $CsPbI_3$ is orthorhombic and therefore it presents an optical anisotropy along the three axis, this property has not been taken into account since the sample is a randomly oriented polycrystalline layer.

3. Results and discussion

As described in the experimental section, the starting $CsPbI_3$:5Eu film was obtained by spin-coating and annealing at 80 °C and then cooling down to 30 °C (0.5 °C–1 °C s^{-1}). As a result, a LT-γ black phase was produced, similarly to what was done in [44].

Our experiment consists of measuring the phase change of the starting layer along the thermal cycle sketched in figure 1, with the single measurement at a certain temperature taking 15 min (*in situ* isochronal and isothermal analyses).

The overall thermal cycle was planned to try to capture and analyse some milestone phases reported in literature [10, 27, 44, 46] for thick and thin layers or powders but never attempted on thin films (∼80 nm) with Europium as additive, and in particular a low temperature (LT) γ-black phase, the yellow δ-phase, a high temperature (HT) α-black phase, and finally a HT γ-black phase after quenching the cubic α-phase from high temperature.

As the temperature of the $CsPbI_3$:5Eu film is increased again to 80 °C, the LT γ-black phase is transformed to yellow δ-phase (hereafter shown and discussed in more details), and remains in that phase up to 280 °C. At 325 °C the film changes from yellow δ to HT-α black phase. When the HT-α black is slowly cooled from 325 °C to RT, the yellow δ-phase is formed again. In figure 2(a), we show the x-ray diffraction patterns of the LT-γ black, HT-α black and yellow δ-phases formed *in situ* during analysis under N_2 using an heating stage, with diagnostic peaks identified by the related Miller indexes. In particular we observe that: the LT-γ black phase is univocally defined by the overlap of three peaks in the region $2\theta = 19.5$–$21°$; the HT-α black phase has four peaks in the overall range that match with a cubic phase having $a = 0.63$ nm; the yellow δ-phase contributes with peculiar peaks, especially at $2\theta = 9.88°$ and $2\theta = 13.10°$.

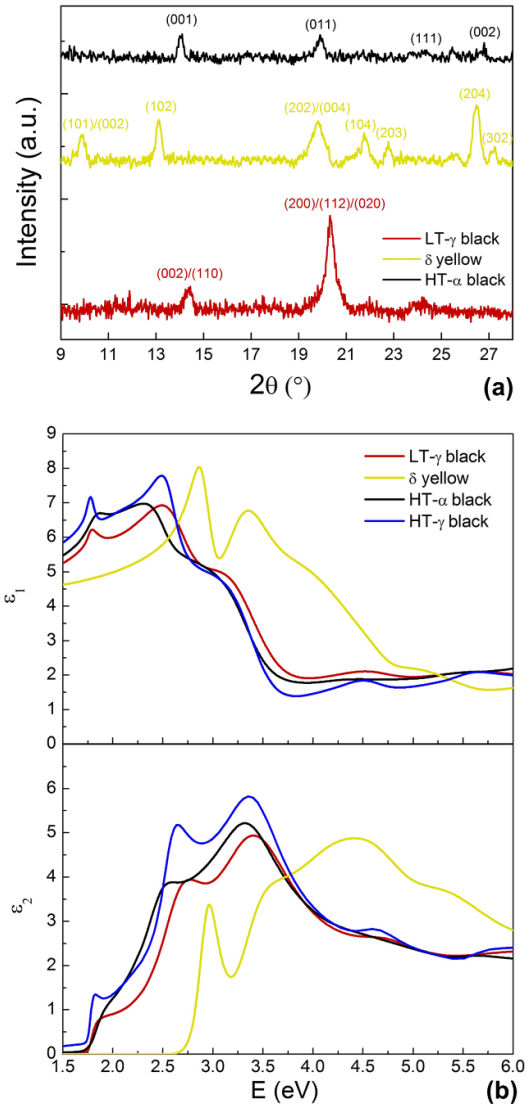

Figure 2. *In situ* results: XRD patterns and characteristic peaks with their Miller indexes of LT-γ black, δ yellow and HT-α black (a). *In situ* results: real and imaginary part of the dielectric function of the three black phases (LT-γ black, HT-α black and HT-γ black) and the yellow phase (δ yellow) (b).

A similar *in situ* experiment was done at the spectroscopic ellipsometer, wherein the sample was likewise kept under N_2 while changing its temperature using an heating stage. The dielectric function of the three phases LT-γ black, HT-α black and the yellow δ-phase are shown in figure 2(b).

An alternative quenching pathway was defined in a recent work [27, 46] wherein it was shown that an orthorhombic γ-black phase can be obtained by a fast quenching of the α-black phase from 350 °C to RT. In this case, the black phase is kinetically frozen thanks to the strain induced in the $CsPbI_3$ thin film [47]. The method was previously applied to powders, thick and thin layers (>200 nm) of $CsPbI_3$ without additives or using HI. In a similar way, we have quenched the HT-α black film from 325 °C to RT in our ellipsometer setup which is equipped with a closed-circle circuit into which liquid nitrogen is pumped to cool the sample at an average rate >100 °C min^{-1} (up to 150 °C min^{-1} in the first minute). Figure 2(b) shows the dielectric function of this phase in comparison to the other three phases (LT-γ black, HT-α black and of the yellow δ-phase). From the comparison of the line profiles (shape and position of the features) emerges that the quenched phase is an orthorhombic γ-black phase (HT-γ black).

Although the two black orthorhombic phases (HT and LT) bear the same crystallographic structure, similarities and differences can be highlighted in the range 2–4 eV (figure 2(b)). In particular, the HT-γ black phase shows a slightly higher absorption with respect to the LT-γ black phase. According to the fitting procedure, the perovskite thickness slightly varied from 72 nm (γ-LT) to 68 nm (γ-HT) as measured at RT likewise the surface roughness decreased from 5 nm (γ-LT) down to 2 nm (γ-HT), thus denoting a slight densification of the layer upon annealing. Nonetheless, the two curves have a very similar shape in terms of

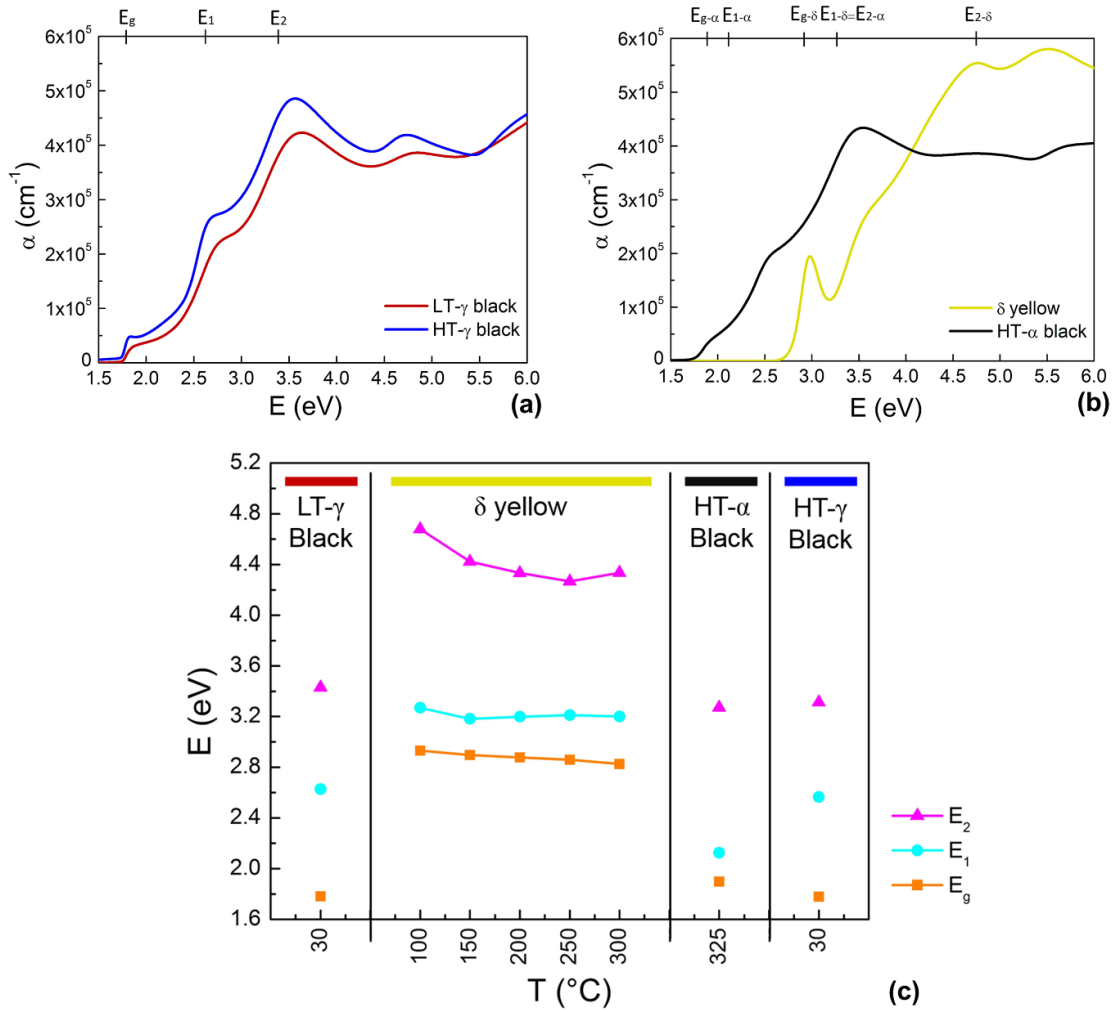

Figure 3. Absorption coefficient (α $_{cm-1}$) as a function of the photon energy (E_{eV}) for (a) LT γ—black and HT γ-black phases; (b) δ-yellow and HT α-black phases. (c) Trend of the energy gap (E_g), the second (E_1) and the third (E_2) critical point values of $CsPbI_3$ (Eu/Pb = 5%) layers during the thermal cycle. The all data are taken on the same sample along the thermal cycle depicted in figure 1, and indeed can be straightforwardly compared.

peaks and valleys in the absorption coefficient α (cm^{-1}) figure 3(a) that has been calculated from the real (ε_1) and imaginary (ε_2) parts of the dielectric function using the formula [48]:

$$\alpha = \frac{2E}{c\hbar}\sqrt{\frac{\sqrt{\varepsilon_1^2+\varepsilon_2^2}-\varepsilon_1}{2}} \tag{1}$$

where E is the photon energy, c is the speed of light in vacuum and $\hbar$ is the reduced Planck constant. The absorption coefficient of the HT-α black phase compared to that of the non-photoactive δ yellow phase is drastically different as depicted in figure 3(b).

For a deeper understanding of the optical behaviour of the film along the transition path with a univocal criterion, we extracted the critical points (CPs) that are associated to specific optical transitions into the material. This approach, initially used by Cardona *et al* [49, 50] for semiconductors, has been recently extended to perovskites. We have recently used the same formalism to quantitatively and thoroughly describe degradation of perovskites and temperature evolution of inter-band transitions in bulk perovskites [51, 52].

The real (ε_1) and imaginary (ε_2) part of the dielectric function of the material mirror the electronic band structure. By fitting simultaneously, the second derivatives of the real part ε_1 and the complex part ε_2 [49, 50], the CP of the joint density of states, which represent the inter-band allowed transitions, is usually extracted. The overall fitting function is the sum of several functions, one for each CP's, described by the equation [53]:

$$\frac{\partial^2\varepsilon}{\partial\omega^2} = n(n-1)Ae^{i\Phi}(\omega - E + i\Gamma)^{(n-2)} \text{ for } n \neq 0 \tag{2}$$

Table 1. Values of E_g, E_1 and E_2 critical points with the related error bar of fitting for LT-γ black at 30 °C, δ-yellow phase at 100 °C, HT-α black at 325 °C and HT γ-black phases as extracted from the critical point analysis.

	LT-γ black	δ-yellow @100 °C	HT-α black	HT-γ black
E_g (eV)	1.781 ± 0.001	2.932 ± 0.001	1.897 ± 0.001	1.779 ± 0.001
E_1 (eV)	2.628 ± 0.003	3.268 ± 0.003	2.125 ± 0.002	2.565 ± 0.003
E_2 (eV)	3.43 ± 0.03	4.68 ± 0.01	3.27 ± 0.02	3.39 ± 0.02

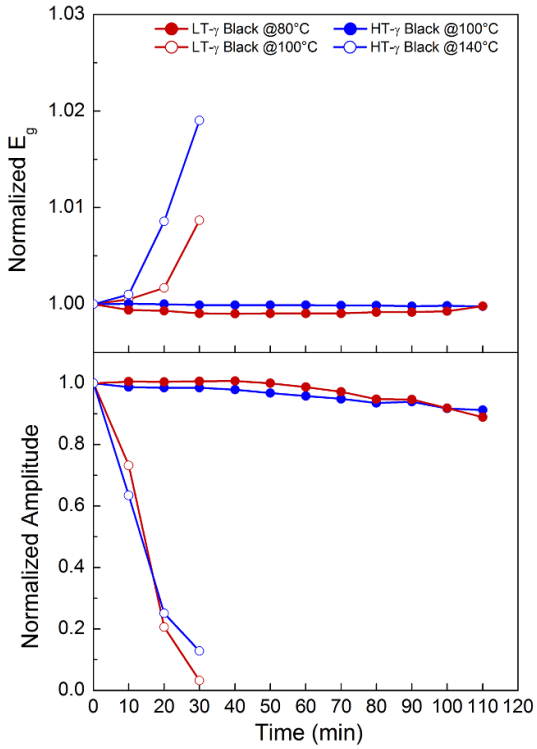

Figure 4. Black phase thermal stability evaluated by stress tests in terms of the evolution over the time of E_g and of the related amplitude A, calculated by CPs analysis, normalized to the respective values at t = 0 for the LT-γ–black phase at 80 °C and 100 °C, and for the HT-γ black phase at 100 °C and 140 °C.

where A (eV), Φ, E (eV), Γ(eV) and n are the amplitude, phase, energy position, broadening and the dimensionality of the CP [45]. In general, the exponent n is $-1/2$ for one dimensional, 0 for two dimensional or $1/2$ for three dimensional critical points. When describing excitonic optical transitions, typical of perovskite materials, n is -1, as reported in [54, 55].

Although one can see that the spectra are characterised by five CPs, going from the energy gap (E_g) to higher energy (above 5 eV), the black-yellow-black phase transition can be effectively described by focusing on three of CPs. In figure 3(c), we have indeed represented their trend, i.e. the energy gap (E_g), the second critical point (E_1) and the third critical point value (E_2) varying during the thermal cycle. When the LT-γ black phase moves to the δ-yellow phase, the CP energy positions sharply increase, attesting the huge difference in the two crystallographic structures and the corresponding electronic structures. The values of energy positions of each CP are reported in table 1. An increase in the temperature within the large interval of 100 °C–300 °C only slightly shifts the CP energy. At 325 °C, a sudden change of the CP energy occurs. In particular, all the CP energies move coherently to lower energies, attesting the formation of the α-black phase. This HT-α black phase, however, is not identical to the LT γ-black phase, as attested by the CP energy position reported in table 1 and figure 3(c). As previously reported, if the sample is cooled down slowly (2.5 °C min^{-1}), a δ-yellow phase is formed at the end of the path (30 °C). The only option to change the final state is to cool down the sample as quickly as possible (>100 °C min^{-1}). As a result, the phase formed after this fast quenching (HT-γ phase) has similar inter-band transition energies as the ones of the LT-γ phase (table 1).

An important aspect from the technology point of view is the comparison of the durability of the two γ phases (LT and HT) in order to eventually validate the use of low-temperature processes to form the black phase. This evaluation is done through a stress test by monitoring the optical response *in situ* during prolonged exposure at a given temperature. They are indeed accelerated ageing tests for which we used N_2

environment to explore the thermodynamic intrinsic stability of the two materials [51]. The temperatures are chosen above the maximum thermal working condition of a solar cell (∼65 °C). As a criterion, we used the change over time of the γ-phase critical point energy (E_g) and its amplitude (A in equation (2)), as calculated by the CPs analysis. As shown in figure 4, the trend of E_g and A, normalized to the values measured at $t = 0$, are strictly related. When the black phase begins to transform into yellow phase, it is observed that: (a) the amplitude, which accounts for the amount of the black γ-phase in the sample, decreases; (b) E_g increases. We found that at 100 °C, the HT-γ black phase is stable whereas the LT-γ black phase turns to yellow after 30 min. Increasing the temperature up to 140 °C, the HT-γ black phase degrades quickly and it turns to yellow after 20–30 min. On the other hand, the LT-γ black phase hugely extends its stability at 80 °C, being comparable to those of the HT-γ black phase at 100 °C. We argue that the differences between the LT-γ black and the HT-γ black resides in an improvement of lattice order occurring in HT-γ black when it is heated up to high temperature (325 °C). Nonetheless, the good stability achieved by LT-γ black under thermal stress at 80 °C (higher than the working temperature of a solar cell) demonstrates that this phase can be considered a feasible solution for photovoltaic application. Furthermore, this comparative study allows opening a viable perspective for the LT-γ black phase to be used in device architectures that needs low thermal budget in the process flowchart such as tandem solar cells.

4. Conclusions

The phase evolution of $CsPbI_3$ thin films (∼80 nm) prepared with an Eu/Pb ratio = 5%, has been monitored during the thermal cycle 30 °C–325 °C–30 °C by in situ spectroscopic ellipsometry measurements and investigated by CPs analysis. Structural identification has been supported by in-situ x-ray diffraction analyses. The use of thin layers has allowed revealing the mainstays and the intrinsic behaviour of the material with respect to what is known for thick and thin layers without additives, powders and single crystals.

The initial orthorhombic black LT-γ phase, obtained by annealing the $CsPbI_3$:5Eu at T = 80 °C for 1 min, converts to the yellow δ-phase when the temperature is increased to 100 °C and above. The yellow δ-phase, which drastically differs from the black phases in structure and optical properties, changes to the cubic HT-α phase at T = 325 °C. Starting from that, an orthorhombic γ-black phase structure (HT-γ black) is reformed by rapid quenching (∼100 °C min^{-1}) to RT, similar to what previously reported in literature for films without additives or using HI [27, 47]. If the cooling speed is not high enough, an orthorhombic yellow δ-phase is instead formed. The HT-γ and LT-γ black phases have similar inter-band transition energies, but they differ for the absorption intensity in the range 2–4 eV and for the behaviour under isothermal stress testing. In particular, under accelerated ageing test in nitrogen environment at T = 100 °C, the HT-γ black is stable within the time of analyses (110 min) as opposed to the LT-γ phase that fully transforms to δ-yellow after ∼30 min. On the other hand, at T = 80 °C the LT-γ phase extends its stability window and behaves similarly to the HT-γ phase at T = 100 °C. This result indeed encourages the use of the LT-γ phase under typical thermal working conditions of solar cells (∼65 °C).

Besides providing optical parameter baselines to discriminate the different phases, we disclosed that, from the technological viewpoint, the LT-γ phase represents a viable solution to be applied in monolithic tandem solar cells compared to the unfeasible γ–phase formed at HT.

Data availability statement

All data that support the findings of this study are included within the article (and any supplementary files).

Acknowledgments

The project was partially supported by the bilateral project on Perovskite Solar Cells (CUP B56C18001070005), co-founded by CNR (Italy) and JSPS (Japan). CNR gratefully acknowledges the project PON entitled 'Tecnologia per celle solari bifacciali ad alta Efficienza a 4 terminali per utility scale', called BEST-4U, financed by the Italian Ministry MIUR (CUP B88D19000160005) and the Project PON ARS01_01007 entitled EleGaNTe Electronics on GaN-based Technologies (CUP B91G18000200005).

ORCID iDs

Salvatore Valastro https://orcid.org/0000-0002-1297-4174
Giovanni Mannino https://orcid.org/0000-0003-2196-6309
Antonino La Magna https://orcid.org/0000-0002-4087-5210
Alessandra Alberti https://orcid.org/0000-0002-4103-6208

References

[1] Leijtens T, Bush K A and Prasanna R 2018 *Nat. Energy* **3** 828
[2] Wali Q, Elumalai N K, Iqbal Y, Uddin A and Jose R 2018 *Renew. Sustain. Energy Rev.* **84** 89
[3] National Renewable Energy Laboratory (NREL) Best Research-Cell Efficiency Chart (Available at: www.nrel.gov/pv/cell-efficiency.html) (Accessed 01 December 2020)
[4] Alberti A, Bongiorno C, Smecca E, Deretzis I, La Magna A and Spinella C 2019 *Nat. Commun.* **10** 2196
[5] Alberti A, Smecca E, Sanzaro S, Mannino G, Deretzis I and La Magna A 2019 *Riv. Nuovo Cimento* **42** 301
[6] Smecca E, Numata Y, Deretzis I, Pellegrino G, Boninelli S, Miyasaka T, La Magna A and Alberti A 2016 *Phys. Chem. Chem. Phys.* **18** 13413
[7] Valastro S *et al* 2020 *Energies* **13** 3953
[8] Shirayama M, Kato M, Miyadera T, Sugita T, Fujiseki T, Hara S, Kadowaki H, Murata D, Chikamatsu M and Fujiwara H 2016 *J. Appl. Phys.* **119** 115501
[9] Abdelmageed G, Jewell L, Hellier K, Seymour L, Luo L, Bridges F, Zhang J Z and Carter S 2016 *Appl. Phys. Lett.* **109** 233905
[10] Marronnier A, Roma G, Boyer-Richard S, Pedesseau L, Jancu J M, Bonnassieux Y, Katan C, Stoumpos C C, Kanatzidis M G and Even J 2018 *ACS Nano* **12** 3477
[11] Yao H, Zhao J, Li Z, Ci Z and Jin Z 2021 *Mater. Chem. Front.* **5** 1221
[12] Jena A K, Kulkarni A and Miyasaka T 2019 *Chem. Rev.* **119** 3036
[13] Fu Y *et al* 2017 *Chem. Mater.* **29** 8385
[14] Wang P, Zhang X, Zhou Y, Jiang Q, Ye Q, Chu Z, Li X, Yang X, Yin Z and You J 2018 *Nat. Commun.* **9** 2225
[15] Li B, Zhang Y, Fu L, Yu T, Zhou S, Zhang L and Longwei Y 2018 *Nat. Commun.* **9** 1076
[16] Li Z, Yang M, Park J, Wei S, Berry J J and Zhu K 2016 *Chem. Mater.* **28** 284
[17] Nam J K, Chai S U, Cha W, Choi Y J, Kim W, Jung M S, Kwon J, Kim D and Park J H 2017 *Nano Lett.* **17** 2028
[18] Bai D, Zhang J, Jin Z, Bian H, Wang K, Wang H, Liang L, Wang Q and Liu S F 2018 *ACS Energy Lett.* **3** 970
[19] Lau C F J *et al* 2018 *J. Mater. Chem.* A **6** 5580
[20] Liang J, Zhao P, Wang C, Wang Y, Hu Y, Zhu G, Ma L, Liu J and Jin Z 2017 *J. Am. Chem. Soc.* **139** 14009
[21] Sutton R J *et al* 2016 *Adv. Energy Mater.* **6** 1502458
[22] Duan J, Zhao Y, Yang X, Wang Y, He B and Tang Q 2018 *Adv. Energy Mater.* **8** 1802346
[23] Xiang S, Li W, Wei Y, Liu J, Liu H, Zhu L, Yang S and Chen H 2019 *iScience* **15** 156
[24] Bett A J *et al* 2017 *Energy Proc.* **124** 567
[25] Zhao B *et al* 2018 *J. Am. Chem. Soc.* **140** 11716
[26] Ye Q, Zhao Y, Mu S, Gao P, Zhang X and You J 2019 *Sci. China Chem.* **62** 7
[27] Sutton R J, Filip M R, Haghighirad A A, Sakai N, Wenger B, Giustino F and Snaith H J 2018 *ACS Energy Lett.* **3** 1787
[28] Luo P, Xia W, Zhou S, Sun L, Cheng J, Xu C and Lu Y 2016 *J. Phys. Chem. Lett.* **7** 3603
[29] Wang Y, Zhang T, Kan M and Zhao Y 2018 *J. Am. Chem. Soc.* **140** 12345
[30] Zhang T, Dar M I, Li G, Xu F, Guo N, Grätzel M and Zhao Y 2017 *Sci. Adv.* **3** 1700841
[31] Wang Q, Zheng X, Deng Y, Zhao J, Chen Z and Huang J 2017 *Joule* **1** 371
[32] Yi C *et al* 2020 *Nat. Commun.* **11** 4736
[33] Zhang Y, Yang Y, Zhang X, Wang T, Nian L, Rong Q, Zhou G and Li N 2020 *Org. Electron.* **87** 105940
[34] Yang F, Hirotani D, Kapil G, Kamarudin M A, Ng C H, Zhang Y, Shen Q and Hayase S 2018 *Angew. Chem., Int. Ed.* **57** 12745
[35] Hu Y, Bai F, Liu X, Ji Q, Miao X, Qiu T and Zhang S 2017 *ACS Energy Lett.* **2** 2219
[36] Zhang J, Yang L, Liu R and Chen L 2019 *Mater. Res. Express* **6** 105529
[37] Lau C F J *et al* 2017 *ACS Energy Lett.* **2** 2319
[38] Murugadoss G, Thangamuthu R, Kumar M R and Ravishankar R 2019 *Micro Nano Lett.* **14** 1385
[39] Zhao H, Xu J, Zhou S, Li Z, Zhang B, Xia X, Liu X, Dai S and Yao J 2019 *Adv. Funct. Mater.* **29** 1808986
[40] Swarnkar A, Marshall A R, Sanehira E M, Chernomordik B D, Moore D T, Christians J A, Chakrabarti T and Luther J M 2016 *Science* **354** 92
[41] Sim K M, Swarnkar A, Nag A and Chung D S 2018 *Laser Photonics Rev.* **12** 1700209
[42] Xiang W *et al* 2019 *Joule* **3** 205
[43] Yang R X and Tan L Z 2020 *J. Chem. Phys.* **152** 034702
[44] Jena A K, Kulkarni A, Sanehira Y, Ikegami M and Miyasaka T 2018 *Chem. Mater.* **30** 66684
[45] Mannino G, Deretzis I, Smecca E, La Magna A, Alberti A, Ceratti D and Cahen D 2020 *J. Phys. Chem. Lett.* **11** 2490
[46] Straus D B, Guo S and Cava R J 2019 *J. Am. Chem. Soc.* **29** 11435
[47] Steele J A *et al* 2019 *Science* **365** 679
[48] Fox M 2010 *Optical Properties of Solids* (Oxford: Oxford University Press)
[49] Cardona M 1969 *Solid State Physics: Advances in Research and Applications. Modulation Spectroscopy Supplement 11* (New York: Academic)
[50] Cardona M and Yu P 2010 *Fundamentals of Semiconductors, Physics and Materials Properties* (Berlin: Springer)
[51] Alberti A, Deretzis I, Mannino G, Smecca E, Giannazzo F, Listorti A, Colella S, Masi S and La Magna A 2019 *Adv. Energy Mater.* **9** 1803450
[52] Deretzis I, Smecca E, Mannino G, La Magna A, Miyasaka T and Alberti A 2018 *J. Phys. Chem. Lett.* **9** 3000
[53] Lautenschlager P, Garriga M, Logothetidis S and Cardona M 1987 *Phys. Rev.* B **35** 9174
[54] Fano U 1961 *Phys. Rev.* **124** 1866
[55] Jiang Y, Soufiani A M, Gentle A, Huang F, Ho-Baillie A and Green M A 2016 *Appl. Phys. Lett.* **108** 061905